Acta Materialia 186 (2020) 415–424

Contents lists available at ScienceDirect

Acta Materialia

journal homepage: www.elsevier.com/locate/actamat

Full length article

Shuffle-nanodomain regulated strain glass transition in Ti-24Nb-4Zr-8Sn alloy

Qianglong Liang[a,b,c], Dong Wang[a,*], Yufeng Zheng[b,c,d,**], Shuangshuang Zhao[a], Yipeng Gao[c], Yulin Hao[e], Rui Yang[e], Dipankar Banerjee[f], Hamish L. Fraser[b,c], Yunzhi Wang[b,c,***]

[a] Center of Microstructure Science, Frontier Institute of Science and Technology, State Key Laboratory for Mechanical Behavior of Materials, Xi'an Jiaotong University, Xi'an, Shaanxi 710049, China
[b] Department of Material Science and Engineering, Center for the Accelerated Maturation of Materials (CAMM), The Ohio State University, 2041 College Rd., Columbus, OH 43210, USA
[c] Department of Materials Science and Engineering, The Ohio State University, Columbus, Ohio, USA
[d] Department of Chemical and Materials Engineering, University of Nevada Reno, 1664N. Virginia St., Reno, NV 89557, USA
[e] Shenyang National Laboratory for Materials Science, Institute of Metal Research, Chinese Academy of Science, Shenyang, Liaoning, China
[f] Department of Materials Engineering, Indian Institute of Science, Bengaluru, Karnataka 560012, India

ARTICLE INFO

Article History:
Received 25 June 2019
Revised 30 December 2019
Accepted 30 December 2019
Available online 6 January 2020

Keywords:
Ti-alloys
Superelasticity
Martensitic transformation
Nano-confinement
in-situ transmission electron microscopy

ABSTRACT

The unprecedented properties of multi-functional metastable β-Ti alloys, including superelasticity over a wide temperature range, ultra-low modulus, and Invar and Elinvar anomalies, have attracted a great deal of attention. Persistent research efforts have been made towards the understanding of the origins of these unique properties. In this article we report a novel shuffle-nanodomain regulated strain glass transition in a metastable β-Ti alloy, Ti-24Nb-4Zr-8Sn (wt.%, Ti2448), which could be the dominant transformation pathway that offers these unique properties. Using the *ex-situ* aberration-corrected scanning transmission electron microscopy and *in-situ* cooling transmission electron microscopy, we find that randomly distributed $\{011\}\langle 0\bar{1}1\rangle_{\beta}$ O′ phase (orthorhombic, shuffle only) nanodomains embedded in the β phase (BCC) matrix at room temperature transform to α'' phase (orthorhombic) with a continuous increase in the amount of $\{2\bar{1}1\}\langle \bar{1}\bar{1}1\rangle_{\beta}$ shear upon cooling or loading. Crystallographic analysis shows that the shuffle of the O′ phase will restrain the twelve possible shears that transform a BCC lattice to α'' martensite to only two. Thus, the randomly distributed O′ nanodomains prevent the formation of long-range-ordered, self-accommodating transformation-strain domain patterns seen in normal martensitic transformations and suppress completely the sharp first-order, auto-catalytic and avalanche-like martensitic transformation into a high-order-like (continuous) strain glass transition. Such a continuous β → O′ → α'' strain glass transition has been confirmed by dynamic mechanical analysis, resistivity and differential scanning calorimetric measurement. This unique transition pathway allows us to offer new insights into the unique properties found in this alloy.

1. Introduction

Due to its unprecedented mechanical and physical properties, such as superelasticity [1], ultra-low modulus [2,3], high strength and ductility [2], excellent biocompatibility [4], and tunable thermal expansion [5], the multi-functional metastable β titanium alloy, Ti-24Nb-4Zr-8Sn (wt.%, Ti2448), has become an excellent candidate for many advanced biomedical applications [6], such as orthopedic implants [7], broken spine/ankle bones repair [8], biomedical scaffolds [9], etc. However, a lack of comprehensive understanding of the key mechanisms underlying these unique properties limits significantly the optimization of the alloy for specific applications. Among the various mechanisms proposed more recently to explain the nearly linear superelastic behavior of Ti2448, one critical factor in common is martensitic transformation. For example, by performing *in-situ* straining TEM [1], X-ray diffraction [10], and synchrotron X-ray diffraction analysis [11], Hao et al. proposed that stress-induced martensitic transformation plays an important role in the nearly linear recoverable strain behavior exhibited by the alloy through a reversible β → α'' martensitic transformation under loading and unloading. Liu et al. reported stress-induced reversible B2 to α'' and BCC to δ (orthorhombic) martensitic transformations at

* Corresponding author.
** Corresponding author at: Department of Chemical and Materials Engineering, University of Nevada Reno, 1664N. Virginia St., Reno, NV 89557, USA.
*** Corresponding author at: Department of Material Science and Engineering, Center for the Accelerated Maturation of Materials (CAMM), The Ohio State University, 2041 College Rd., Columbus, OH 43210, USA.
E-mail addresses: wang_dong1223@xjtu.edu.cn (D. Wang), yufengz@unr.edu (Y. Zheng), wang.363@osu.edu (Y. Wang).

https://doi.org/10.1016/j.actamat.2019.12.056
1359-6454/

nanoscale via TEM and *in-situ* synchrotron X-ray diffraction and have attributed them to the origin of superelasticity of the Ti2448-0.1O alloy [12,13]. However, normal martensitic transformations are strongly first-ordered and take place in an autocatalytic and avalanche fashion, generating highly non-linear superelasticity within a rather narrow temperature range (<50 K) [14,15], which cannot account for the nearly linear superelastic behavior of Ti2448 over a wide temperature range (~500 K) [5]. Although Liu et al. noticed that the martensitic transformations in Ti2448 occur at nanometer scales [12,13], no analysis on possible phase transformation pathways leading to such nanodomains of martensite has been offered yet.

Most recently, a concentration modulation at nanoscale in Ti2448 has been reported by using the atom probe tomography analysis [5,16]. The unique superelastic behavior of the alloy over a wide temperature range [5,16–19], as well as the Invar and Elinvar anomalies [5,16,20] have been attributed to the confined martensitic transformation by such nanoscale concentration modulations. However, in addition to the nanoscale concentration modulations reported in [5,16], more recent studies have shown ample evidences of nanoscale structural non-uniformities in as-quenched states of various metastable β titanium alloys, including Ti-26Nb-2Zr (at%) [21,22], Ti-18Mo (wt%) [23,24], Ti-18Mo-5Al (wt%) [25], and Ti-4Al-4Fe-0.25Si-0.1O (wt%) [26], in particular, nanodomains of an orthorhombic structure referred to as O′ phase. O′ has also been observed and distinguished unambiguously from the α'' martensite in Ti2448 [27].

The transformation from β to either hexagonal α' martensite in solute lean alloys of titanium or orthorhombic α'' martensite in β stabilized alloys on rapid quenching is based on the Burgers orientation relationship [28]. It is accomplished mechanistically by a $\{2\bar{1}1\}\langle 11\bar{1}\rangle_\beta$ shear and a $\{011\}\langle 0\bar{1}1\rangle_\beta$ shuffle, and can follow either of two transformation pathways in which either the shuffle precedes the shear or the shear precedes the shuffle as shown in Fig. 1 [21,29]. The α'' martensite results from a partial shear and shuffle and has an intermediate structure in relation to α'. The stability of the α'' phase and the degrees of the shear and shuffle involved in the β to α'' transformation can be influenced significantly by alloy composition [30–32]. Banerjee et al. explained the formation of "stacking domains" in α' and α'' martensite through a pathway of shear followed by shuffle [33]. When the shuffle precedes the shear, the process can be arrested after the shuffle (for reasons that will be discussed later in the paper) and the resultant structure has been designated as the O′ phase. This alternative transformation path was first postulated in order to explain the anomalous result that Al decreases the Ms temperature in β stabilized alloys [33] although the T_0 temperature (at which the free energy between the α and β phases are equal) should increase with Al addition since Al is an α stabilizer. A systematic study of various compositions was carried out to isolate and identify the O′ phase [21,23,25,27]. Both experimental characterization [21,23,25,27] and computational calculations using density function theory [24] have shown that the O′ phase can form in metastable β titanium alloys when the concentration of substitutional solutes, such as β phase stabilizer Mo, Nb and α phase stabilizer Al, exceed a critical value, and that the O′ phase formation can be accelerated significantly by altering the content of interstitial solutes such as oxygen [25]. It has been reported that the presence of the O′ phase could influence the deformation behavior of metastable β titanium alloys, such as the type of the deformation twins in Ti2448 [34]. However, whether such an O′ nanodomain structure sets the stage for nanodomains of martensite, that is the second segment of the transformation path, has not been investigated. Furthermore, due to the limitations of the conventional characterization techniques, the degree of shear and the degree of shuffle involved in the β to α'' transformation have not been quantified, which significantly hindered the understanding of the actual transformation pathway that is responsible for the nearly linear superelastic behavior of the alloy.

In this study, we couple differential scanning calorimetry (DSC) measurement, resistivity measurement, dynamic mechanical analysis (DMA), and *in-situ* cooling transmission electron microscopy (TEM) and ex-situ aberration-corrected high-angle annular dark field scanning

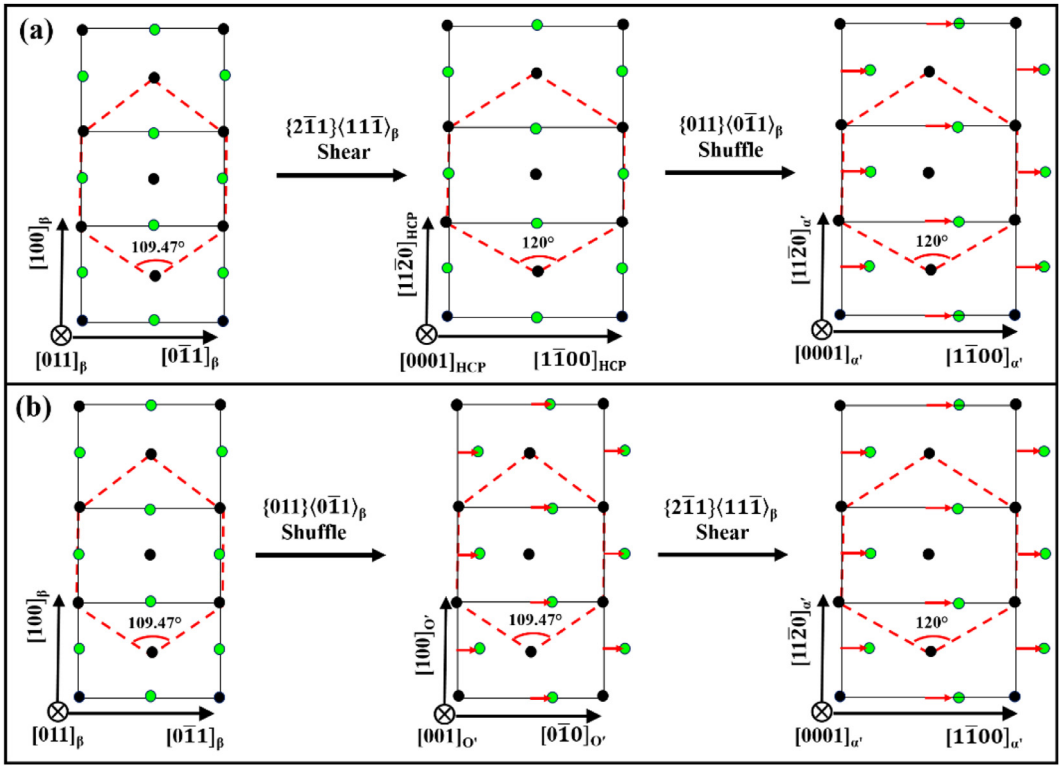

Fig. 1. Schematic drawing of the two different transition pathways in titanium alloys from parent β phase (BCC) to α' martensite phase (HCP) transition involving $\{011\}\langle 0\bar{1}1\rangle_\beta$ shuffle and $\{2\bar{1}1\}\langle 11\bar{1}\rangle_\beta$ shear: (a) Transition pathway showing $\{2\bar{1}1\}\langle 11\bar{1}\rangle_\beta$ shear followed by $\{011\}\langle 0\bar{1}1\rangle_\beta$ shuffle; (b) Transition pathway showing $\{011\}\langle 0\bar{1}1\rangle_\beta$ shuffle followed by $\{2\bar{1}1\}\langle 11\bar{1}\rangle_\beta$ shear, with O' phase as an intermediate state phase.

transmission electron microscopy (HAADF-STEM) techniques with crystallographic and thermodynamic analyses to investigate phase transformation pathways in Ti2448 during cooling from room temperature to liquid nitrogen temperature and during cold rolling to study the effect of O′ nanodomains on the formation of α''. We first show that in the solution treated and quenched samples, normal (i.e., strong first-order) martensitic transformation is absent as indicated by the DSC measurement and nanodomains of orthorhombic structure are formed by the electrical resistivity measurement and *ex-situ* aberration-corrected S/TEM. Instead, a strain glass transition [35] is revealed by DMA measurement. Using the HAADF-STEM, isolated and randomly distributed O′ nanodomains are observed. These nanodomains continuously transform to α'' nanodomains with increased lattice shear upon cooling in a wide temperature range from room temperature (RT) to 87 K, evaluated by *in-situ* cooling TEM characterization, and upon loading observed by the HAADF-STEM imaging in the 50% cold-rolled Ti2448 samples. Crystallographic analysis shows that the shuffle within the O′ phase nanodomains allows a single nanodomain of O′ to transform to only two of twelve possible variants of α'' martensite. Thus, the O′ nanodomains provide a precursor to martensite in which one component of the martensitic transformation is accomplished within the nanodomain and this accomplished shuffle component restricts the martensite variants that can form within a single nanodomain.Thus O′ phase confines the martensitic transformation to each nanodomain, changing the Landau free energy landscape from a typical first-order transformation into a higher-order (continuous) transformation. Our work provides the first unambiguous experimental evidence that distinguishes the shuffle from the shear during BCC to orthorhombic structure transformation in Ti2448, suggesting a novel transformation pathway of $\beta \rightarrow O' \rightarrow \alpha''$ shuffle-nanodomain regulated strain glass transition, which offers new insights into the mechanisms underlying the unique properties of the Ti2448 alloy.

2. Experimental methods

The ingot of Ti2448 alloy was fabricated in a vacuum arc melter using a Ti-Sn master alloy with pure Ti, Nb and Zr (>99.9% purity) and its actual composition was measured as Ti-24.2Nb-3.96Zr-8.1Sn-0.2O (wt.%) using wet chemical and gas analysis. The samples wrapped with pure titanium foil were solution treated at 1173 K (T_β ~1000 K) for 30 min in a tube furnace followed by water quenching to room temperature. The transformation latent heat was measured by DSC TA Q200 with a heating and cooling rate of 10 K/min. The samples tested using DSC were first heated up from room temperature (293 K) to 473 K and subsequently cooled down to 123 K, followed by being reheated to 473 K. Mechanical susceptibility of Ti2448 was measured by DMA using the TA Q800 equipment in the single cantilever mode, with a continuous cooling rate of 2 K/min, frequency range from 0.2 to 20 Hz, and different static loads from 0 to 100 MPa. The electrical resistivity of Ti2448 was measured using a four-point method with constant current of 100 mA from 525 K to 125 K at cooling rate of 2 K/min in the Instec HCP621GP hot and cold stage under a vacuum environment. The solutionized and quenched Ti2448 sample was cold-rolled to 50% reduction in thickness by 40 passes. The thin foils for TEM analysis were prepared from the center part of the thermal and/or mechanical treated samples, using Dual-Bean Focused Ion Beam (DB-FIB) FEI Helios Nanolab 600 system, and the ion beam damage on the foil surfaces resulting from the DB-FIB was minimized using low voltage Ar^+ ion milling in a Fischione Nanomill™ Model 1040. Selected area diffraction patterns (SADP) and dark field images were collected on the FEI Tecnai G2 30 TEM operated at 300 kV using liquid-nitrogen-cooling holder (Gatan model 636) from room temperature (293 K) to 87 K. Z-contrast HAADF-STEMimaging was conducted on the aberration-corrected FEI Titan3™ 80–300 at 300 kV, using a convergence semi-angle of 12 mrad and a collection semi-angle of 44 mrad, with an incident beam dwell-time of 4 μs/px and a beam current of ≈100 pA. DigitalMicrograph software (version 3.30.2017.0) was used to clean the high-resolution HAADF-STEM images and the ImageJ software (version 1.52k) was used to plot the intensity profiles recorded from the SADP and HAADF-STEM images. The SADP of β, O′, and α'' phases were simulated via CrystalMaker (version 10.4.5) using the lattice parameters reported in Ti2448 [12].

3. Experimental results

3.1. Strain glass transition in Ti2448

The initial microstructure of solutionized and quenched Ti2448 alloy is shown in Fig. 2. In the $[100]_\beta$ zone axis SADP, as shown in Fig. 2(a), additional weak diffraction spots are observed near $^1/_2\{310\}_\beta$, implying the presence of an orthorhombic structure [21]. By selecting one such additional diffraction spot as marked by the red circle, randomly distributed nanodomains are revealed in the interior of the β phase matrix in the dark field image shown in Fig. 2(b). The above characterization of diffraction pattern and dark field imaging are consistent with the observations in previous work [12,13,27], indicating that normal martensite with long-range ordered, self-accommodating domain patterns does not form in Ti2448 during quenching.

The characteristic features of nanodomain formation are further evaluated using DSC, electrical resistivity measurement and DMA, and the results are shown in Fig. 3(a–c). In the heat flow curve measured from DSC shown in Fig. 3(a), neither an exothermic peak upon cooling nor an endothermic dip upon heating has been observed within the temperature range between 473 K and 123 K, revealing the absence of normal martensitic transformation in Ti2448 within this temperature range. However, the measured electrical resistivity (normalized by the value at 293 K) first decreases from 525 K to approximately 350 K, and then increases continuously from approximately 350 K to 125 K, as shown in Fig. 3(b), indicating that a phase transformation occurs around 350 K. This suggests that the observed orthorhombic nanodomains shown in Fig. 2(a and b) initiate in the parent β phase matrix at this temperature. The storage modulus measured using DMA under different frequencies from 0.2 to 20 Hz are shown in Fig. 3(c). The storage modulus (i.e., elastic modulus) first decreases (softening) and then increases (hardening) upon cooling. The dip temperature changes with frequency, indicating a frequency-dependent modulus feature. Such frequency-dependent modulus dips are related to the frozen temperatures at different frequencies of lattice strain in the nanodomains. When the lattice strains in the nanodomains can response to the alternating external force/strain with different frequencies instantaneously, the system is in a pure elastic or dynamic state. When the lattice strains cannot response to

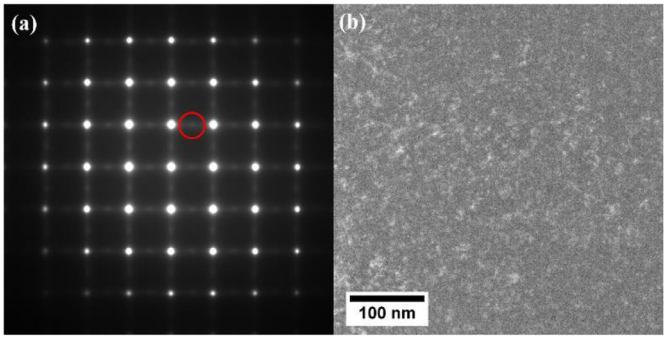

Fig. 2. Microstructure in Ti2448 after being solutionized and quenched to room temperature: (a) $[100]_\beta$ zone axis SADP with additional reflection near $^1/_2\{310\}_\beta$ marked by red color circle and (b) Dark field image by selecting the diffraction marked as red circle in (a) showing the nanodomains of orthorhombic structure present. (For interpretation of the references to colour in this figure legend, the reader is referred to the web version of this article.)

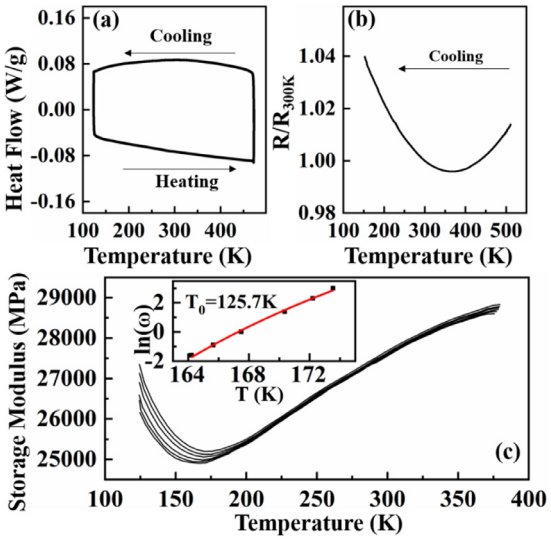

Fig. 3. Transformation characteristics of Ti2448 alloy: (a) DSC heat flow curve showing the absence of exothermic peak or endothermic dip from 473 K to 123 K; (b) Normalized electrical resistivity curves upon cooling from 525 K to 125 K showing phase transformation around 350 K; (c) Multi-frequency DMA analysis showing frequency-dependent modulus with the inset showing the ideal freezing temperature by fitting Vogel-Fulcher relation.

the alternating external force/strain with all frequencies instantaneously, the system is in a viscoelasticitic or frozen state. These observations are the characteristic features of the so-called strain glass transition. Strain glass transition describes a transition from a dynamically disordered lattice strain state (i.e., the austenite, which is in a "strain liquid" state) at high temperature to a static ("frozen") disordered lattice strain state (i.e., a "strain glass" state consisting random nanodomains of martensite) at low temperature with only local strain order [35–37]. These are in contrast to the long-range ordered static lattice strain state (i.e., a "strain crystal" state) found in a internally twinned martensitic plate. The strain glass transition is the ferroelastic counterpart of relaxor transition in ferroelectrics and cluster spin glass transition in ferromagnetics [36,37]. The frequency-dependent dip temperature, T_g, of storage modulus is then fitted using the empirical Vogel-Fulcher relation, $\omega = \omega_0 exp[-E_a/k_B(T_g - T_0^f)]$ [36,38], where ω is the frequency, ω_0 represents the frequency prefactor, E_a is the activation energy, k_B is the Boltzmann constant, T_g describes the strain glass freezing temperature at different frequencies, and T_0^f is the ideal freezing temperature with 0 Hz. The ideal freezing temperature T_0^f obtained by fitting is shown in the inset of Fig. 3(c) and all lattice strains associated with the martensitic transformation (independent of the domain size) are frozen at T_0^f. Thus, our results demonstrate that the normal martensitic transformation is completely suppressed during quenching from above the β transus temperature to room temperature in Ti2448, and a strain glass transition occurs during further cooling from room temperature to 125 K.

The microstructural evolution during the strain glass transition is further analyzed via *in-situ* cooling TEM from room temperature to 87 K, as shown in Fig. 4(a and b). The SADPs and the corresponding dark field images of Ti2448 in $[100]_\beta$ zone axis are recorded from 293 K (room temperature) to 87 K and the results are shown in Fig. 4 (a). At each temperature, the diffraction pattern (top image) and its corresponding dark field image (bottom) are shown in the same column. Apart from the sharp BCC reflections, additional reflections belonging to the orthorhombic phase near $1/2\{013\}_\beta$ are observed at each temperature within the wide temperature range from 293 K to 87 K, and the intensities of the additional reflections are much weaker as compared to those of the BCC reflections. The intensities of these additional reflections were further investigated using the ImageJ software (version 1.52k), and the line intensity profiles along the red color dashed lines in SADP at each temperature are plotted in Fig. 4(b). It is readily seen that upon cooling the intensities of additional reflections belonging to the orthorhombic phase keep increasing from 293 K to 87 K. The dark field images recorded by selecting the additional reflections marked by the red circles show that the nanodomains are stable in a wide range of temperature. It is also seen that the area fraction of these nanodomains and their average size increases continuously upon cooling. Such domain growth is consistent with the continuous intensity increase of additional reflections in the SADP. In conjunction with the above DSC and DMA analyses, we can conclude that a continuous strain glass transition takes place in Ti2448 during cooling from 293 K to 87 K.

Note that the reflections near $^1/_2\{013\}_\beta$ indicating an orthorhombic structure could be attributed either to α'' martensite or O′ phase nanodomains. Thus, it is critical to quantify the degree of shear and shuffle components involved in these nanodomains at different stages during cooling. This has been done by performing direct measurements and analysis from the SADPs and HAADF-STEM images, and is described in the subsequent section.

3.2. Strain glass transition during cooling

In order to unambiguously distinguish the O′ phase from the α'' phase and to quantify the shuffle and shear component in the orthorhombic nanodomains (O′ or α''), aberration-corrected S/TEM technique was adopted and the acquired HAADF-STEM images are analyzed. The structure of the orthorhombic nanodomains at room temperature is characterized from two perpendicular directions, $[100]_\beta$ and $[011]_\beta$, revealed in the filtered HAADF-STEM images by selecting the spatial frequencies in the corresponding fast fourier transforms (FFT) in Fig. 5. Two different variants of the orthorhombic phase are highlighted in the red and blue lines in Fig. 5(a), with the spatial frequencies belonging to these two different variants highlighted in the inset marked by red and blue arrows. The structure of each variant is shown in Fig. 5(b) and (c), respectively, by higher magnification HAADF-STEM images. In one variant labeled as V1, every other $(0\bar{1}1)_\beta$ planes (atoms with green color) shuffle along the $[0\bar{1}\bar{1}]_\beta$ direction, while in the other variant labeled as V2, every other $(011)_\beta$ planes (atoms with green color) shuffle along the $[0\bar{1}1]_\beta$ direction. Thus, these two variants are formed via two different $\{011\}\langle 0\bar{1}1\rangle_\beta$ shuffles. The two shuffles are further validated by the line intensity profiles plotted along the red dashed arrows across the non-shuffled and shuffled atomic columns in the insets of Fig. 5(b and c). The degree of the $\{011\}\langle 0\bar{1}1\rangle_\beta$ shuffle at room temperature is then evaluated by direct measurement of the displacement of atomic columns on every other $(011)_\beta$ planes along the $[0\bar{1}1]_\beta$ direction from the HAADF-STEM image, as shown in Fig. 5(d–f). Fig. 5(d) shows the structure of a nanodomain and Fig. 5(e) shows the displacement of atom columns by plotting line intensity profiles along the red and blue dotted lines in Fig. 5(d). The distance of the atomic shuffle along the $[0\bar{1}1]_\beta$ direction can be quantified using the difference of atomic column intensity peak locations in Fig. 5(e). Based on the Burgers path for the BCC to HCP structural transformation, the atomic shuffle needed to transform BCC lattice to HCP lattice is 16.67% of the interplanar spacing of $d_{(0\bar{1}1)\beta}$. However, the degree of shuffle measured from the nanodomain shown in Fig. 5(e) is only 4% of the interplanar spacing of $d_{(0\bar{1}1)\beta}$, indicating that the atomic shuffle is incomplete in the nanodomains. The degree of shear (represented by the lattice strain in the $[0\bar{1}1]_\beta$ direction) involved in the orthorhombic structure nanodomains at room temperature is then evaluated by measuring the difference between the interplanar spacing of $d_{(0\bar{1}1)\beta}$ in the BCC lattice (Fig. 5(f)) and the lattice parameter, b, of the orthorhombic nanodomain (Fig. 5(d)), from the HAADF-STEM image shown in Fig. 5(g). The quantity of $\zeta = \left(\left(b - d_{(0\bar{1}1)\beta}\right)/d_{(0\bar{1}1)\beta}\right) \times 100\%$ is then used to quantify the amount of shear. The average value of ζ

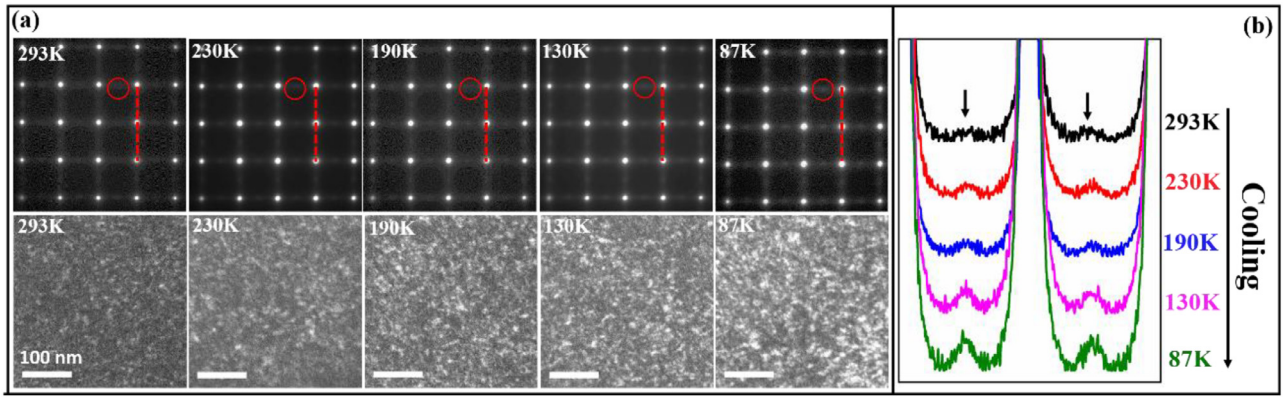

Fig. 4. *In-situ* cooling TEM characterization showing the continuous strain glass transition from 293 K to 87K: (a) The SADPs recorded in $[100]_\beta$ zone axis from 293 K to 87 K and corresponding dark field images showing the continuous growth of nanodomains upon cooling and (b) The line intensity profiles plotted along the red dashed lines in (a) showing a continuous increase of additional reflections (indicated by black color arrows) intensity from 293 K to 87 K. (For interpretation of the references to colour in this figure legend, the reader is referred to the web version of this article.)

is close to zero (within the measurement uncertainty) in the orthorhombic nanodomains. Thus, the characterization using *ex-situ* aberration-corrected S/TEM has provided direct evidence that the orthorhombic structure in the nanodomains found in the as-quenched Ti2448 is the O′ phase formed by a pure shuffle.

To further explore the evolution of these nanodomains upon cooling, the degree of $\{2\bar{1}1\}\langle\bar{1}\,\bar{1}1\rangle_\beta$ shear involved is evaluated by the same parameter $\zeta = \left(\left(b - d_{(0\bar{1}1)\beta}\right)/d_{(0\bar{1}1)\beta}\right) \times 100\%$ via the measurement from the SADPs collected using *in-situ* cooling TEM (Fig. 6(b)). The indices of β, O′ and α'' phases in the diffraction patterns in Fig. 6(b) can be referred to the simulated diffraction patterns of β phase, O′ phase and α'' phase shown in Fig. 6(a) separately using the lattice parameters reported in Ti2448 in Table 1 [12]. The interplanar spacing of $d_{(0\bar{1}1)\beta}$ in BCC lattice is measured by the red dotted line and the lattice parameter, *b*, of the orthorhombic phase, is measured along the blue dotted line, shown in Fig. 6(d). The measured degree of shear increases from nearly zero at room temperature to higher than 1% at 87 K and it keeps increasing upon cooling. The continuous increase of the finite amounts of the $(2\bar{1}1)[\bar{1}\,\bar{1}1]\beta$ shear developed in the nanodomains is consistent with the strain glass transition behavior described in Section 3.1, suggesting a higher-order and continuous transition behavior of O′ → α'' strain glass transition from room temperature to 87 K. Note that the shear value, more specifically, the lattice strain along the $[0\bar{1}1]_\beta$ direction, at different temperatures fits well with Landau theory of second-order transformation as shown by the red dashed curve in Fig. 6(d). The lattice strain of a well-developed α'' phase related to the lattice change of $d_{(0\bar{1}1)\beta}$ in Ti2448 is calculated as ~2.66% using the lattice parameters given in [12], the normalized lattice strain by this value of well-developed α'' upon cooling reaches ~50% down to 0 K.

3.3. Strain glass transition under loading

In order to analyze the influence of external loading on the O′ → α'' strain glass transition, the storage modulus upon cooling

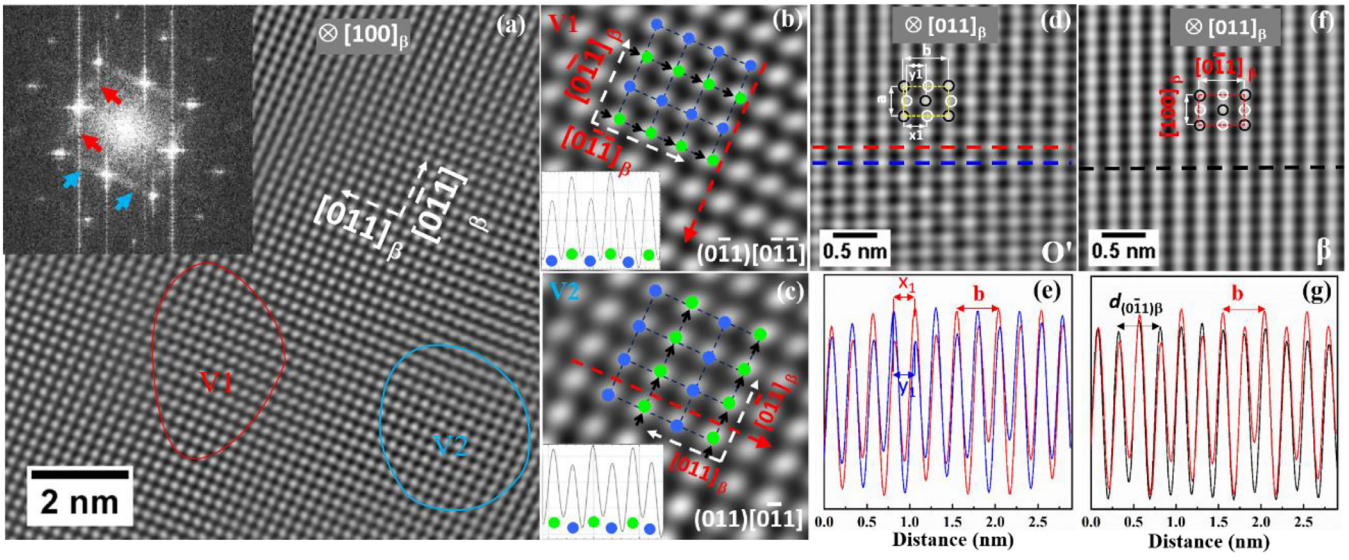

Fig. 5. HAADF-STEM images showing orthorhombic nanodomains at room temperature: (a) HAADF-STEM image recorded with the incident beam parallel to $[100]_\beta$ showing two orthorhombic nanodomains of different variants marked by blue and red color circles with corresponding FFT in the inset highlighting spatial frequencies of two variants by blue and red arrows; (b-c) Higher magnification HAADF-STEM images of two different variants showing $(0\bar{1}1)[0\bar{1}\bar{1}]$ and $(011)[0\bar{1}1]$ shuffle respectively, with shuffled atom columns marked by green circles and non-shuffled atom columns marked by blue circles and insets show the periodic intensity change generated by atomic plane shuffle by plotting the line intensity profiles along the red dashed arrows; (d) HAADF-STEM image acquired with the incident electron beam parallel to $[011]_\beta$ showing orthorhombic nanodomain; (e) Intensity profiles along the red and blue lines in (d) showing the displacement of every other $(011)_\beta$ planes; (f) HAADF-STEM image of BCC matrix recorded with incident electron beam parallel to $[011]_\beta$; (g) Intensity profiles plotted along the black line in (f) and red line in (d) with direction of $[0\bar{1}1]_\beta$, measuring the interplannar spacing difference between $d_{(0\bar{1}1)\beta}$ and b. (For interpretation of the references to colour in this figure legend, the reader is referred to the web version of this article.)

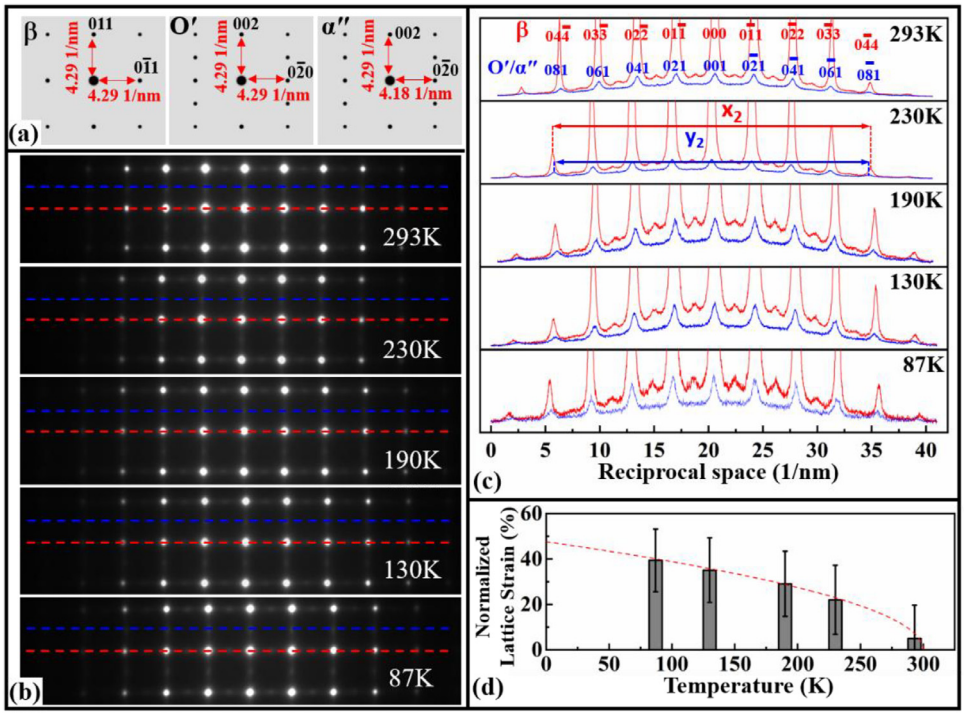

Fig. 6. The measurement of shear component in the nanodomains during cooling by the same parameter $\zeta = \left(\left(b - d_{(0\bar{1}1)\beta}\right)/d_{(0\bar{1}1)\beta}\right) \times 100\%$ using *in-situ* cooling TEM: (a) Simulated $[100]_{\beta}$ zone axis SADP for β phase, $[011]_{O'}$ zone axis SADP for O' phase and $[011]_{\alpha''}$ zone axis SADP for α'' phase using the reported lattice parameter in Ti2448 in Table 1 [12]; (b) Recorded $[100]_{\beta}$ zone axis diffraction patterns in Ti2448 from 293 K to 87 K via *in-situ* cooling TEM; (c) Intensity profiles of the red and blue lines in (b), showing the reflections belonging to β phase and O' (or α'') phase; (d) Measured and fitted shear induced strain from 293 K to 87 K. (For interpretation of the references to colour in this figure legend, the reader is referred to the web version of this article.)

is measured using DMA under three different pre-loading stresses, 20 MPa, 50 MPa and 100 MPa, and with various frequencies from 0.2 Hz to 20 Hz. The results are shown in Fig. 7(a-c). All the results show the same trends of the storage modulus change with temperature and the frequency dependence of the dip temperature, which indicate a strain glass transition behavior similar to that shown in the measurement without loading (shown in Fig. 3(c)). Clear modulus softening and broad dip of storage modulus with frequency dependence are detected upon cooling, suggesting that loading up to 100 MPa could not convert the strain glass transition to martensitic transformation. In addition, the ideal freezing temperature, T_0^f, obtained by fitting the dip temperature T_g in the Vogel-Fulcher (VF) equation, increases from 129.6 K to 141.3 K when the load increases from 20 MPa to 100 MPa, indicating that the external load favors the O′ → α'' strain glass transition.

Table 1
The lattice parameters in Ti2448 in [12] used for the SADP simulations.

Phase	*a* (Å)	*b* (Å)	*c* (Å)
β	3.298	3.298	3.298
α''	3.222	4.788	4.667
O' (theoretical)	3.298	4.664	4.664

The microstructure in the 50% cold-rolled Ti2448 is investigated using aberration-corrected S/TEM technique and the results are shown

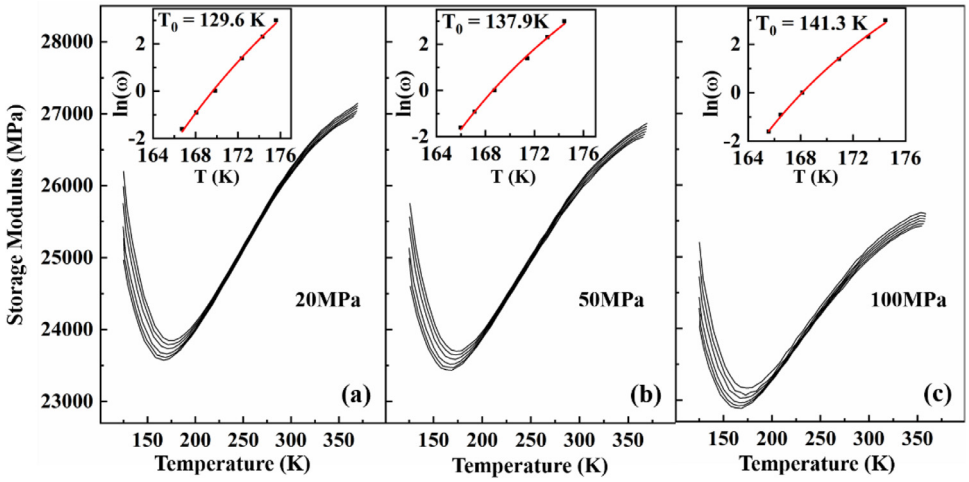

Fig. 7. Strain glass transition characteristic by multi-frequency DMA analysis with different pre-loading stress: Multi-frequency (0.2Hz~20 Hz) dependent storage modulus with pre-loading stress of 20Mpa (a), 50 MPa (b), and 100 MPa (c). Strain glass freezing temperature T_0^f at different pre-loading stresses are obtained by fitting the dip temperatures through Vogel-Fulcher relation as shown in insets.

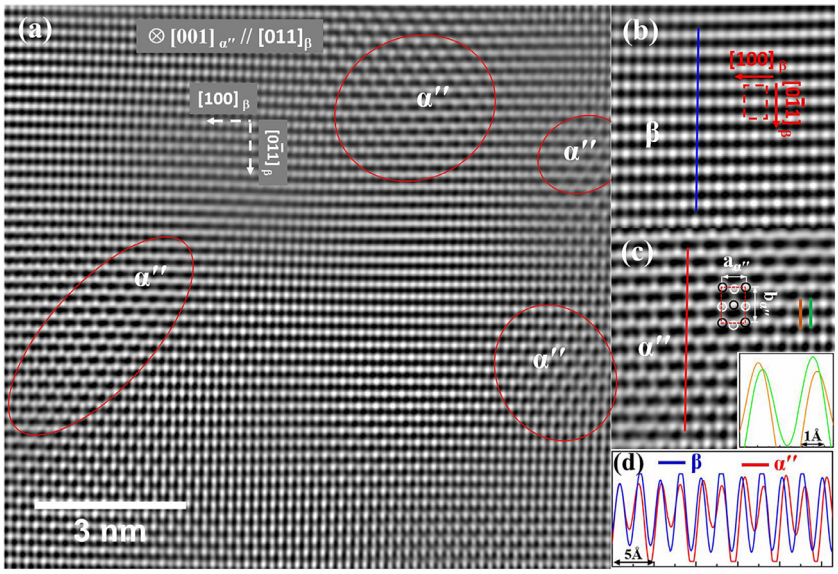

Fig. 8. HAADF-STEM image showing α'' martensitic nanodomains in 50% cold rolled Ti2448: (a) HAADF-STEM image recorded with the incident beam along $[011]_\beta$ direction indicating α'' martensitic nanodomains marked by red color circles; (b-c) HAADF-STEM images showing the structure of β matrix and α'' nanodomain with inset of (c) showing the line profile of orange and green lines within α'' domain area, suggesting shuffle displacement. (d) The line intensity profiles along blue and red color lines in (b) and (c) showing the plane spacing differences generated by lattice shear. (For interpretation of the references to colour in this figure legend, the reader is referred to the web version of this article.)

in Fig. 8(a–d). In the HAADF-STEM image recorded with the incident beam parallel to $[011]_\beta$, isolated nanodomains of orthorhombic structure are observed (marked by red circles in Fig. 8(a)). In order to determine whether the nanodomains belong to O′ or α'', the degree of shuffle and the degree of shear in the nanodomains are evaluated using HAADF-STEM images in Fig. 8(b–d), adopting the same method discussed in Section 3.2 (Fig. 5). The degree of shuffle in the nanodomains in Fig. 8(c) (the orange and green lines and related intensity profile of the inset in Fig. 8(c)) is determined to be 5.1%, slightly larger than that in the O′ phase (~4.0%) in the as-quenched state before deformation, while the degree of shear is determined to be 2.3% (through the intensity profile shown in Fig. 8(d)), significantly higher than that in the O′ phase. Therefore, the observed nanodomains in the 50% cold rolled Ti2448 belong to α'' phase, which is consistent with our previous observation of nanoscale α'' phase in the 10% cold rolled Ti2448 [34]. Such α'' nanodomains in the 50% cold rolled Ti2448 are believed to form under confinement within the pre-formed O′ nanodomains before deformation.

4. Discussion

4.1. O′ → α″ strain glass transition

Compared with the β → α'' [1,39,40] and β → δ [12,13] martensitic transformations reported previously, our experimental results suggest a novel transformation pathway during cooling from above the β transus temperature to room temperature and then further cooling to 87 K, i.e.,

$$\beta \rightarrow O' \rightarrow \alpha''.$$

In particular, the observations using conventional TEM and aberration-corrected S/TEM have shown nanoscale O′ phase of orthorhombic structure in solutionized and quenched Ti2448, which is consistent with the β → O′ transformation (a pure shuffle transformation) pathway systematically reported in our previous work [21, 23,25–27]. Further, the absence of heat flow peak in the DSC measurement and the storage modulus dip shown at low temperature in the DMA suggest a continuous strain glass transition from O′ → α'' upon further cooling from room temperature. This has been confirmed by *in-situ* cooling characterization, which has shown a continued increase in the amount of $\{2\bar{1}1\}\langle\bar{1}\bar{1}1\rangle_\beta$ shear upon cooling from room temperature to 87 K, quantified by an increased lattice strain along the $[0\bar{1}1]_\beta$ direction. The $\{2\bar{1}1\}\langle\bar{1}\bar{1}1\rangle_\beta$ shear develops in the O′ shuffle-nanodomains and the degree of such shear keeps increasing with the growth of the O′ nanodomains upon cooling, as supported by the increased intensity and the peak shift of the orthorhombic reflections and increases in the volume fraction and size of nanodomains shown in Fig. 4(a and b). Thus, the transformation pathway upon cooling from room temperature to 87 K can be concluded as the following: the quenched-in O′ shuffle-nanodomains continue to grow upon cooling, and is accompanied by simultaneous development of the $\{2\bar{1}1\}\langle\bar{1}\bar{1}1\rangle_\beta$ shear in these shuffle-nanodomains. The latter component transforms the O′ nanodomains to α'' nanodomains. Although we cannot rule out the possibility for direct formation of some α'' domains from the BCC matrix, the minimum energy pathway should be β → O′ → α'' since the required shuffle for the β → α'' transformation already exists in the O′ domains.

Besides cooling from room temperature to 87 K, the O′ → α'' transformation has also been observed under loading. Firstly, the storage modulus curves measured under increased external loads via DMA show an increase in the dip temperature, suggesting that the external loads favor the O′ → α'' transformation. Secondly, the characterization using *ex-situ* aberration-corrected S/TEM technique shows that before cold-rolling there exists only O′ nanodomains, while after cold-rolling α'' nanodomains with a lattice strain of 2.3% appear. In particular, the α'' nanodomains observed in the cold-rolled samples exhibit similar sizes as those of the O′ nanodomains before cold rolling, indicating that the α'' nanodomains are confined by the O′ nanodomains. In contrast to the reversible O′ to α'' transformation upon cooling and α'' to O′ transformation upon heating, the α'' phase formed by heavy cold rolling (e.g., 50% thickness reduction) is stable. However, it maintains a similar nanodomain structure, due most likely to the same confinement by the O′ nanodomains. It should be pointed out that our previous work using high-energy XRD has shown a continuous change of the diffraction patterns of α'' in Ti2448 upon loading and unloading [12,13], which could be associated with the O′ ↔ α'' transformation during loading and unloading.

We note that the transformation from β to O′ during cooling from above β transus to room temperature has not been characterized directly, apart from the *ex-situ* characterization of O′ phase at room temperature using conventional TEM and aberration-corrected S/TEM. However, the absence of exothermic and endothermic peak in the DSC heat flow curve shown in Fig. 3(a) and the continuous change in resistivity from 500 K to room temperature shown in Fig. 3 (b) may suggests a second-order transition. In addition, our previous *in-situ* heating TEM characterization of another metastable β titanium alloy, Ti-5Al-5Mo-5V-3Cr [41], showed a continuous decrease in the intensity of the O′ phase reflections upon heating from room temperature to around 300 °C, also an indication of a second-order phase transition. Furthermore, it is observed in the HAADF-STEM images (Fig. 5 and Fig. 8) that the degree of shuffle and shear near the nanodomain / β interface region is not the same as that in the interior of the nanodomains, and the degree of shuffle and shear shows a continuous increase from the interface region to the center of the nanodomains. Nevertheless, several unanswered questions remain regarding the nature of the β to O′ transformation. For example, we do not understand what determines the scale of the nanodomain structure and what control the kinetics of the nanodomain formation and coarsening? We also do not understand the role of extremely fine scale compositional variations have been observed in Ti2448 [5,16] via atom probe tomography.

4.2. Crystallographic analysis of O′ → α″ strain glass transition

In the preceding section we have shown that the O′ nanodomains formed upon quenching after solution treatment can serve as a precursor for the formation of α″ martensite during subsequent cooling or loading. Such an O′ → α″ transformation is distinctively different from the normal autocatalytic martensitic transformation; it preserves the nanodomain structure and does not show any of the signatures of a normal martensitic transformation such as heat flow peaks in DSC measurements. Instead, it shows all the characteristic features of a typical strain glass transition [35–37], such as frequency dependent storage modulus in DMA and the lack of heat flow peaks in DSC. In this section, we carry out a detailed crystallographic analysis to explain how the precursory $\{011\}\langle 0\bar{1}1\rangle_\beta$ shuffle nanodomains regulate the subsequent $\{2\bar{1}1\}\langle \bar{1}\bar{1}1\rangle_\beta$ shear during O′ → α″ transformation, rendering a high-order like, continuous strain glass transition.

As has been mentioned earlier, the O′ and α″ phases share the same orthorhombic symmetry. β → O′ and β → α″ transformations both require the same type of atomic shuffle, i.e., $\{011\}\langle 0\bar{1}1\rangle_\beta$. As distinct from the β → O′ transformation, the β → α″ transformation also requires the $\{2\bar{1}1\}\langle \bar{1}\bar{1}1\rangle_\beta$ shear. When the $\{011\}\langle 0\bar{1}1\rangle_\beta$ shuffle occurs in advance, it will restrict the possibilities of different $\{2\bar{1}1\}\langle \bar{1}\bar{1}1\rangle_\beta$ shear systems to form α″ martensite as shown in Fig. 9. Fig. 9(a) shows the β phase (BCC) lattice structure with a projection viewing along the $[011]_\beta$ direction in the inset. There are six equivalent $\{011\}_\beta$ planes in a BCC lattice and on each $\{011\}_\beta$ plane atoms can shuffle along two opposite $\langle 0\bar{1}1\rangle_\beta$ directions, leading to twelve different $\{011\}\langle 0\bar{1}1\rangle_\beta$ shuffle directions in total. As an example, one of these twelve shuffles, $(011)[0\bar{1}1]_\beta$ is shown in Fig. 9(b), where atoms on every other $(011)_\beta$ planes shuffle along the $[0\bar{1}1]_\beta$ direction, with a projection viewing along the $[011]_\beta$ direction given in the inset. There are twelve equivalent $\{2\bar{1}1\}_\beta$ planes that can shear in $\langle \bar{1}\bar{1}1\rangle_\beta$ directions, leading to twelve different shears. However, under the condition that one of the twelve $\{011\}\langle 0\bar{1}1\rangle_\beta$ shuffle occurs first, the $\{2\bar{1}1\}\langle \bar{1}\bar{1}1\rangle_\beta$ shear will be reduced from 12 down to 2, as summarized in Table 2. For example, once the $(011)[0\bar{1}1]_\beta$ shuffle described in Fig. 9(b) occurs first, only $(2\bar{1}1)[\bar{1}\bar{1}1]_\beta$ and $(21\bar{1})[\bar{1}1\bar{1}]_\beta$ shear can occur to form the α″ phase, as shown in Fig. 9 (c). As indicated in the projection along $[011]_\beta$ (lower left inset in Fig. 9(c)), the shear occurs in the rhombus cell marked as green with the shear plane $(2\bar{1}1)$ projected onto the purple lines and the shear direction $[\bar{1}\bar{1}1]_\beta$ marked as blue arrows, leading to an orthorhombic symmetry with **a, b** and **c** perpendicular to each other, as illustrated by the projections along the three perpendicular directions, $[011]_\beta$, $[100]_\beta$ and $[0\bar{1}1]_\beta$. If another type of $\{2\bar{1}1\}\langle \bar{1}\bar{1}1\rangle_\beta$ shear occurs, such as $(211)[\bar{1}11]_\beta$, after the $(011)[0\bar{1}1]_\beta$ shuffle shown in Fig. 9(d), the BCC lattice will transform to a monoclinic structure rather than an orthorhombic structure, because the shuffled atoms (green) are out of the $(0\bar{1}1)_\beta$ plane as shown in the $[0\bar{1}1]_\beta$ projection (the lower right inset in Fig. 9(d)). The monoclinic structure with a non-90° γ angle between **a** and **c** is shown by a parallelogram cell colored green in Fig. 9(d), with the shear plane projected into the purple lines and the shear directions indicated by the blue arrow.

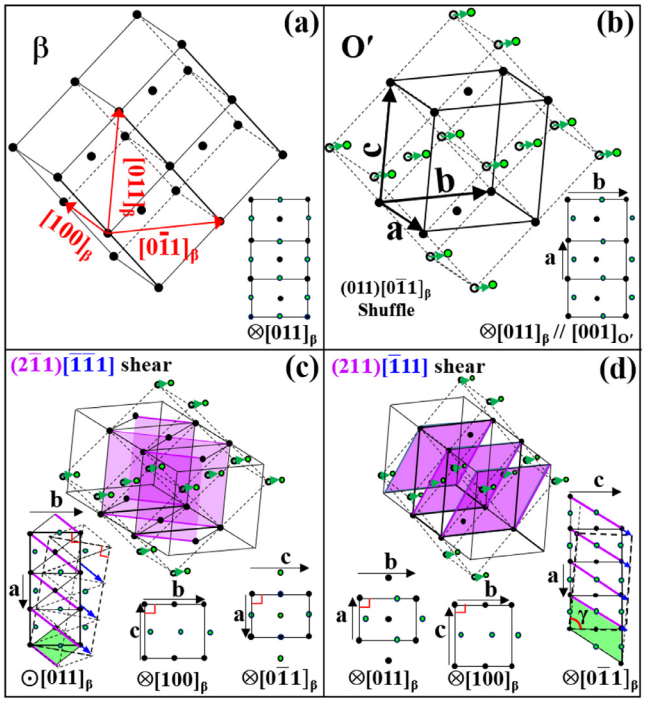

Fig. 9. Qualitative crystallography analysis of confined shuffle-nanodomain regulated α″ strain glass transition. Base vectors are defined as $[\bar{1}00]_\beta//[100]_{O'}//[100]_{\alpha''}$; $[0\bar{1}1]_\beta//[010]_{O'}//[010]_{\alpha''}$; $[011]//[001]_{O'}//[001]_{\alpha''}$: (a) β phase with BCC structure and its projection in $[011]_\beta$ direction, with green and black circles representing atoms on the adjacent $(011)_\beta$ planes; (b) $(011)[0\bar{1}1]_\beta$ shuffle generated O′ phase with orthorhombic structure and its projection in $[011]_\beta$ direction, with green circles indicating the shuffled atoms on every other $(011)_\beta$ planes along $[0\bar{1}1]_\beta$ direction marked using green arrows; (c) $(011)[0\bar{1}1]_\beta$ shuffle regulated $(2\bar{1}1)[\bar{1}\bar{1}1]_\beta$ shear and its projection in $[011]_\beta$, $[100]_\beta$ and $[0\bar{1}1]_\beta$ directions; (d) $(011)[0\bar{1}1]_\beta$ shuffle regulated $(211)[\bar{1}11]_\beta$ shear and its projection in $[011]_\beta$, $[100]_\beta$ and $[0\bar{1}1]_\beta$ directions. (For interpretation of the references to colour in this figure legend, the reader is referred to the web version of this article.)

4.3. Thermodynamic analysis of O′ to α″ strain glass transition

The above crystallographic analysis is supportive of the experimental observation of O′ to α″ shuffle-nanodomain regulated strain glass transition. The regulation is enforced by the restraint of the precursor $\{011\}\langle 0\bar{1}1\rangle_\beta$ shuffle on the subsequent $\{2\bar{1}1\}\langle \bar{1}\bar{1}1\rangle_\beta$ shear. To analyze the continuous O′ to α″ transformation behavior in contrast to a normal martensitic transformation from an energetic point of view, we draw schematically the Landau free energy curves for both cases in Fig. 10. Fig. 10(a) shows the typical Landau free energy curves at different temperatures for a first-order martensitic transformation, where a discrete jump of lattice shear as the order parameter

Table 2
Shuffle-regulated shears for each shuffle to transform BCC structured β phase to orthorhombic α'' phase.

Shuffle plane	Shuffle direction	Shear Mode	
(011)	$[01\bar{1}]$	$(2\bar{1}1)[\bar{1}11]$	$(21\bar{1})[\bar{1}1\bar{1}]$
	$[0\bar{1}1]$		
$(01\bar{1})$	[011]	$(211)[\bar{1}11]$	$(2\bar{1}\bar{1})[\bar{1}1\bar{1}]$
	$[0\bar{1}\bar{1}]$		
(101)	$[10\bar{1}]$	$(\bar{1}21)[\bar{1}11]$	$(12\bar{1})[1\bar{1}\bar{1}]$
	$[\bar{1}01]$		
$(10\bar{1})$	[101]	$(\bar{1}2\bar{1})[\bar{1}1\bar{1}]$	$(121)[1\bar{1}1]$
	$[\bar{1}0\bar{1}]$		
(110)	$[1\bar{1}0]$	$(\bar{1}12)[\bar{1}1\bar{1}]$	$(1\bar{1}2)[1\bar{1}\bar{1}]$
	$[\bar{1}10]$		
$(1\bar{1}0)$	[110]	$(\bar{1}\bar{1}2)[\bar{1}1\bar{1}]$	$(112)[11\bar{1}]$
	$[\bar{1}\bar{1}0]$		

occurs during the transformation upon cooling. Fig. 10(b) shows the Landaus free energy curves corresponding to a high-order continuous transformation, where the equilibrium order parameter (lattice shear, corresponding to the minimum of the free energy) as a function of temperature changes continuously. The change of the overall transformation characteristics from first-order to higher-order could be attributed to the constraint enforced by and the precursor effect from the O′ nanodomains. Only limited shearing directions for the formation of α'' martensite can be realized in the O′ nanodomains and no self-accommodation could be accomplished within a single nanoscale shuffle domain. Because of the random spatial distribution of the O′ nanodomains, no self-accommodation could be accomplished among the α'' domains either. This continuous transition feature has eliminated temperature or stress plateau on the temperature/stress – strain curve. In the meantime, the non-self-accommodating single variant martensitic nanodomains have higher energy and is more difficult to form as compared to a self-accommodated, long-range ordered poly-twin martensitic structure (with same volume) [42, 43] and, thus, requires deeper quenching. On the other hand, as an important component of the α'' phase, the shuffle in the precursory O′ nanodomains may have brought the crystal structure to an embryonic stage of the α'' phase, which can grow continuously upon cooling, accompanied by a continued increase in the degree of shear, as have been evidenced by the above experimental observations (see, e.g., Fig. 6(d)). Therefore, with the O′ nanodomains serving as a regulator as well as a precursor, the Landau free energy minimum shown in Fig. 10(b) shifts continuously from zero to finite strains upon cooling, leading to a continuous transformation.

4.4. O′ to α″ shuffle-nanodomain regulated strain glass transition and related properties in Ti2448

The highly regulated transformation pathway of O′ to α'' could provide new insights regarding the origins of the nearly linear superelasticity over a wide temperature range, as well as the Invar and Elinvar anomalies seen in Ti2448. The *in-situ* TEM characterization and DMA analysis in the current work have shown a continuous transformation from O′ to α'' at nanoscale with continuously increased shear components upon cooling. The shuffle-regulated α'' nanodomains with different amount of shear have been observed to exist within a wide range of temperatures. The degree of lattice shear in the α'' nanodomains increases upon further loading and returns to their initial values upon unloading, offering superelasticity over a wide temperature range. Such an explanation is consistent with the previous study via *in-situ* synchrotron X-ray diffraction, where a continuous increase of lattice strain under external loading was observed [12,44]. After cold rolling, α'' variants with their shear components favored by the external stress grow continuously upon cooling. This continuous transformation of selected variants could generate strain and soften the elastic modulus, which compensate normal contraction and modulus hardening upon cooling and, thus, lead to the Invar and Elinvar anomalies in Ti2448 [5,16,20]. In addition, this formation of O′ and the confined O′ to α'' transition could also help us to understand the stress induced twinning [34,40].

5. Conclusion

In this study, we have discovered a novel O′ → α'' shuffle-nanodomain regulated strain glass transition using a variety of *ex-situ* and *in-situ* characterization techniques, including DSC, electrical resistivity measurement, DMA, *in-situ* cooling TEM and aberration-corrected HAADF-STEM. Nanodomains of an orthorhombic O′ phase have been observed in the solutionized and quenched Ti2448, which are formed by pure atomic shuffle of every other $\{011\}_\beta$ atomic planes along the $\langle 0\bar{1}1\rangle_\beta$ directions of the BCC lattice. A continuous transformation from the O′ nanodomains to α'' nanodomains with a continued increase in the amount of shear upon cooling or loading has been revealed by the *in-situ* cooling TEM characterization and DMA analysis. The structure of the O′ and α'' phases in Ti2448 have been distinguished unambiguously using aberration-corrected HAADF-STEM technique. Such a continuous transformation taking place at nanoscale is drastically different from the normal martensitic transformation. The frequency

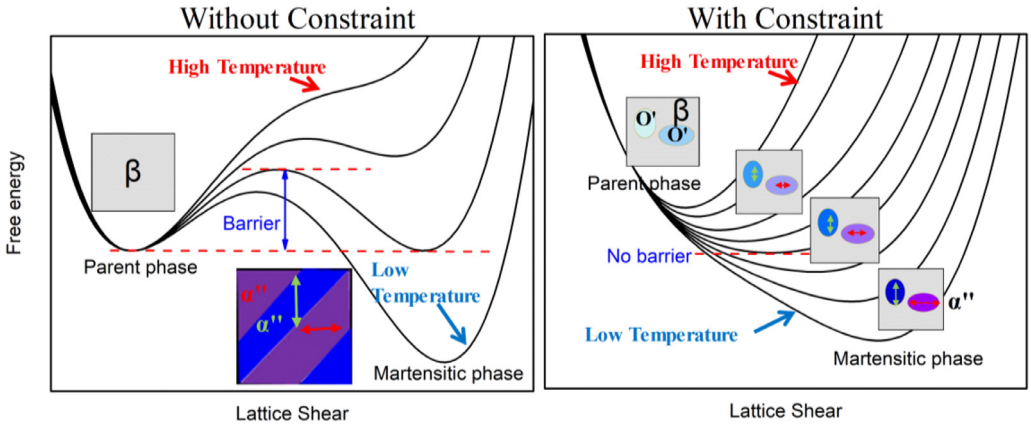

Fig. 10. Landau free energy landscape of martensitic transformation without and with geometric constraint of O' nanodomains: (a) Without constraint, Landau free energy landscape of typical first-order martensitic transformation upon cooling showing energy barrier with a sudden jump of lattice shear during transformation upon cooling, with inset showing internally twined α'' phase; (b) With local constraint caused by O' nanodomains, Landau free energy landscape in O' region upon cooling showing a continuously increased lattice shear without energy barrier, with insets showing microstructure of the β matrix, growing O' nanodomains and α'' nanodomains within O'. The double-headed arrows describe the shear component.

dependent modulus revealed by DMA and the lack of latent heat peak in DSC indicate clearly a strain glass transition. This novel shuffle-nanodomain regulated $O' \rightarrow \alpha''$ strain glass transition could be the key mechanism underlying the unique superelasticity of Ti2448 alloy in a broad temperature range, tunable thermal expansion coefficient, and Invar and Elinvar anomalies.

Declaration of Competing Interest

None.

Acknowledgements

DW acknowledges the support by the National Basic Research Program of China (Grants no. 2016YFB0701302) and the National Natural Science Foundation of China (Grant nos. 51671156, 51501145, 51231008 and 51621063), and IRT13034. QL acknowledges the support from China Scholarship Council (201706280328). YZ, HLF and YW acknowledge the US National Science Foundation DMREF program under grant DMR-1435483. YZ would also like to acknowledge the financial support by the startup funding from the Department of Chemical and Materials Engineering at University of Nevada, Reno. DB acknowledges the Raja Rammana Fellowship.

References

[1] J.P. Cui, Y.L. Hao, S.J. Li, M.L. Sui, D.X. Li, R. Yang, Reversible movement of homogenously nucleated dislocations in a beta-titanium alloy, Phys. Rev. Lett. 102 (2009) 045503.
[2] Y. Hao, S. Li, B. Sun, M. Sui, R. Yang, Ductile titanium alloy with low Poisson's ratio, Phys. Rev. Lett. 98 (2007) 216405.
[3] Y. Hao, S. Li, F. Prima, R. Yang, Controlling reversible martensitic transformation in titanium alloys with high strength and low elastic modulus, Scr. Mater. 67 (2012) 487–490.
[4] Y. Hao, S. Li, S. Sun, C. Zheng, R. Yang, Elastic deformation behaviour of Ti–24Nb–4Zr–7.9 Sn for biomedical applications, Acta Biomater. 3 (2007) 277–286.
[5] Y. Hao, H. Wang, T. Li, J. Cairney, A. Ceguerra, Y. Wang, et al., Superelasticity and tunable thermal expansion across a wide temperature range, J. Mater. Sci. Technol. 32 (2016) 705–709.
[6] L. Wang, L.-.C. Zhang, Development and Application of Biomedical Titanium Alloys, Bentham Science Publishers, 2018.
[7] E. Eisenbarth, D. Velten, M. Müller, R. Thull, J. Breme, Biocompatibility of β-stabilizing elements of titanium alloys, Biomaterials 25 (2004) 5705–5713.
[8] R. Yang, Y. Hao, S. Li, Development and application of low-modulus biomedical titanium alloy Ti2448, Biom. Eng. Tre 10 (2011) 225–247.
[9] Y. Liu, X. Li, L.C. Zhang, T. Sercombe, Processing and properties of topologically optimised biomedical Ti–24Nb–4Zr–8Sn scaffolds manufactured by selective laser melting, Mater. Sci. Eng., A 642 (2015) 268–278.
[10] S. Zhang, S. Li, M. Jia, F. Prima, L. Chen, Y. Hao, et al., Low-cycle fatigue properties of a titanium alloy exhibiting nonlinear elastic deformation behavior, Acta Mater. 59 (2011) 4690–4699.
[11] E. Obbard, Y. Hao, R. Talling, S. Li, Y. Zhang, D. Dye, et al., The effect of oxygen on α'' martensite and superelasticity in Ti–24Nb–4Zr–8Sn, Acta Mater. 59 (2011) 112–125.
[12] J. Liu, Y. Wang, Y. Hao, H. Wang, Y. Wang, Z. Nie, et al., High-energy X-ray diffuse scattering studies on deformation-induced spatially confined martensitic transformations in multifunctional Ti–24Nb–4Zr–8Sn alloy, Acta Mater. 81 (2014) 476–486.
[13] J.-.P. Liu, Y.-.D. Wang, Y.-.L. Hao, Y. Wang, Z.-.H. Nie, D. Wang, et al., New intrinsic mechanism on gum-like superelasticity of multifunctional alloys, Sci. Rep. 3 (2013) 2156.
[14] K. Otsuka, X. Ren, Physical metallurgy of Ti–Ni-based shape memory alloys, Prog. Mater. Sci. 50 (2005) 511–678.
[15] J. Kim, H. Kim, T. Inamura, H. Hosoda, S. Miyazaki, Shape memory characteristics of Ti–22Nb–(2–8) Zr (at.%) biomedical alloys, Mater. Sci. Eng. A 403 (2005) 334–339.
[16] H. Wang, Y. Hao, S. He, T. Li, J. Cairney, Y. Wang, et al., Elastically confined martensitic transformation at the nano-scale in a multifunctional titanium alloy, Acta Mater. 135 (2017) 330–339.
[17] J. Zhu, Y. Gao, D. Wang, J. Li, T.-.Y. Zhang, Y. Wang, Making metals linear superelastic with ultralow modulus and nearly zero hysteresis, Mater. Horiz. 6 (2019) 515–523.
[18] J. Zhu, H. Wu, D. Wang, Y. Gao, H. Wang, Y. Hao, et al., Crystallographic analysis and phase field simulation of transformation plasticity in a multifunctional β-Ti alloy, Int. J. Plast 89 (2017) 110–129.
[19] J. Zhu, Y. Gao, D. Wang, T.-.Y. Zhang, Y. Wang, Taming martensitic transformation via concentration modulation at nanoscale, Acta Mater. 130 (2017) 196–207.
[20] L. Zhang, D. Wang, X. Ren, Y. Wang, A new mechanism for low and temperature-independent elastic modulus, Sci. Rep. 5 (2015) 11477.
[21] Y. Zheng, R.E. Williams, S. Nag, R. Banerjee, H.L. Fraser, D. Banerjee, The effect of alloy composition on instabilities in the β phase of titanium alloys, Scr. Mater. 116 (2016) 49–52.
[22] E. Pang, E. Pickering, S. Baik, D.N. Seidman, N. Jones, The effect of zirconium on the omega phase in Ti-24Nb-[0–8] Zr (at.%) alloys, Acta Mater. 153 (2018) 62–70.
[23] Y. Zheng, D. Banerjee, H.L. Fraser, A nano-scale instability in the β phase of dilute Ti–Mo alloys, Scr. Mater. 116 (2016) 131–134.
[24] M. Li, X. Min, K. Yao, F. Ye, Novel insight into the formation of α''-martensite and ω-phase with cluster structure in metastable Ti-Mo alloys, Acta Mater. 164 (2019) 322–333.
[25] Y. Zheng, T. Alam, R. Banerjee, D. Banerjee, H.L. Fraser, The influence of aluminum and oxygen additions on intrinsic structural instabilities in titanium-molybdenum alloys, Scr. Mater. 152 (2018) 150–153.
[26] S. Lee, C. Park, J. Hong, J.-t. Yeom, The role of nano-domains in {1011} twinned martensite in metastable titanium alloys, Sci. Rep 8 (2018) 11914.
[27] Q. Liang, Y. Zheng, D. Wang, Y. Hao, R. Yang, Y. Wang, et al., Nano-scale structural non-uniformities in gum like Ti-24Nb-4Zr-8Sn metastable β-Ti alloy, Scr. Mater. 158 (2019) 95–99.
[28] W. Burgers, On the process of transition of the cubic-body-centered modification into the hexagonal-close-packed modification of zirconium, Physica 1 (1934) 561–586.
[29] D. Banerjee, J. Williams, Perspectives on titanium science and technology, Acta Mater. 61 (2013) 844–879.
[30] A. Pathak, S. Banumathy, R. Sankarasubramanian, A. Singh, Orthorhombic martensitic phase in Ti–Nb alloys: a first principles study, Comput. Mater. Sci 83 (2014) 222–228.
[31] M. Bönisch, M. Calin, L. Giebeler, A. Helth, A. Gebert, W. Skrotzki, et al., Composition-dependent magnitude of atomic shuffles in Ti–Nb martensites, J. Appl. Crystallogr. 47 (2014) 1374–1379.
[32] W. Mei, J. Sun, Y. Wen, Martensitic transformation from β to α' and α'' phases in Ti–V alloys: a first-principles study, J. Mater. Res. 32 (2017) 3183–3190.
[33] D. Banerjee, K. Muraleedharan, J. Strudel, Substructure in titanium alloy martensite, Philos. Mag. A 77 (1998) 299–323.
[34] Q. Liang, Z. Kloenne, Y. Zheng, D. Wang, S. Antonov, Y. Gao, et al., The role of nano-scaled structural non-uniformities on deformation twinning and stress-induced transformation in a cold rolled multifunctional β-titanium alloy, Scr. Mater. 177 (2020) 181–185.
[35] S. Sarkar, X. Ren, K. Otsuka, Evidence for strain glass in the ferroelastic-martensitic system Ti(50-x)Ni(50+x), Phys. Rev. Lett. 95 (2005) 205702.
[36] X. Ren, Y. Wang, Y. Zhou, Z. Zhang, D. Wang, G. Fan, et al., Strain glass in ferroelastic systems: premartensitic tweed versus strain glass, Philos. Mag. 90 (2010) 141–157.
[37] D. Wang, Y. Wang, Z. Zhang, X. Ren, Modeling abnormal strain states in ferroelastic systems: the role of point defects, Phys. Rev. Lett. 105 (2010) 205702.
[38] M. JA, Spin Glasses, Taylor & Francis, London, 1993.
[39] R. Talling, R. Dashwood, M. Jackson, D. Dye, On the mechanism of superelasticity in Gum metal, Acta Mater. 57 (2009) 1188–1198.
[40] Y. Yang, G. Li, G. Cheng, H. Wang, M. Zhang, F. Xu, et al., Stress-introduced α'' martensite and twinning in a multifunctional titanium alloy, Scr. Mater. 58 (2008) 9–12.
[41] Y. Zheng, S. Antonov, Q. Feng, R. Banerjee, D. Banerjee, H.L. Fraser, Shuffle-induced modulated structure and heating-induced ordering in the metastable β-titanium alloy, Ti-5Al-5Mo-5V-3Cr, Scr. Mater. 176 (2020) 7–11.
[42] T. Waitz, T. Antretter, F. Fischer, N. Simha, H. Karnthaler, Size effects on the martensitic phase transformation of NiTi nanograins, J. Mech. Phys. Solids 55 (2007) 419–444.
[43] M. Lin, G.B. Olson, M. Cohen, Homogeneous martensitic nucleation in Fe-Co precipitates formed in a Cu matrix, Acta Metall. et Mater. 41 (1993) 253–263.
[44] Y. Yang, P. Castany, M. Cornen, F. Prima, S. Li, Y. Hao, T. Gloriant, Characterization of the martensitic transformation in the superelastic Ti–24Nb–4Zr–8Sn alloy by in situ synchrotron X-ray diffraction and dynamic mechanical analysis, Acta Mater. 88 (2015) 25–33.